Bonding Mechanism in Ultrasonic Gold Ball Bonds on Copper Substrate

I. LUM, J.P. JUNG, and Y. ZHOU

The effects of process parameters on bond formation in thermosonic gold ball bonding on a copper substrate at ambient temperatures have been investigated with scanning electron microscopy (SEM). A model was developed based on classical microslip theory to explain the general phenomena observed in the evolution of bond footprints left on the substrate. The specific effects of ultrasonic energy and complex stress distributions arising from tool geometry must be taken into consideration and were incorporated into the model. It was shown that relative motion existed at the bonding interface as microslip at lower powers, transitioning into gross sliding at higher powers. With increased normal bonding forces, the transition point into gross sliding occurred at higher ultrasonic bonding powers.

I. INTRODUCTION

WIRE bonding is the most utilized technique for making microelectronic interconnects from an integrated circuit (IC) to the substrate. Currently, on an annual basis, more than 4 trillion wire bonds are made.[1] It is the flexibility and cost effectiveness of wire bonding that makes it widely accepted in industry. Among the variations of wire bonding techniques (i.e., ball and wedge bonding), the predominant method used today is thermosonic ball bonding of gold wire onto aluminum metallization. Thermosonic ball bonding utilizes a normal bond force simultaneously with thermal and ultrasonic energy to form the first bond (ball) on the IC, followed by the second bond (crescent) on the substrate. However, despite its wide industry acceptance, there is a lack of a quantitative understanding of the bonding mechanisms.[1]

Aluminum is the metallization typically used for thermosonic ball bonding. With the greater demand in microelectronics for ever-increasing clock speeds, methods need to be found to accommodate this trend. Copper possesses much better electrical properties than aluminum, such as lower electrical resistance[2] and the ability to support increased signal speeds. However, there are problems with bonding on copper. Copper forms an oxide layer at the elevated temperatures of thermosonic bonding, which hinders bonding.[3] Although an oxide layer also forms on aluminum, it does not pose a problem for bonding, as it is brittle and easily breaks up and is dispersed.[1] On the other hand, the oxide that forms on copper is soft and, hence, does not fracture, which poses problems for bonding. However, researchers have shown that it is possible to produce reliable bonds on copper using a shielding-gas atmosphere[4] or by bonding at ambient temperatures.[5] In a development study of gold ball bonding on a copper substrate at ambient temperatures,[5] it was found that optimal bonding in terms of bond shape and bond shear force was obtained at a bonding power, force, and time of 325 mW, 35 gf, and 1000 ms, respectively.

At present, a quantitative understanding of the bonding mechanisms is lacking and, specifically, there are no published studies of the bonding mechanisms in gold ball bonding on a copper substrate. Therefore, this study was undertaken to gain a better understanding of the role of process parameters in the ball-bond formation in thermosonic gold ball bonding on a copper substrate at ambient temperatures. The bond footprints left on the substrate were observed with scanning electron microscopy (SEM) for microwelded regions and changes in substrate surface morphology.

A. *Technical Background*

It is widely accepted that wire bonding is a solid-state process.[6] Various evidence to support this includes bonds made at liquid-nitrogen temperatures[7] and studies of the bond interface with transmission electron microscopy (TEM).[8] One of the requirements to form metallurgical bonding is a relatively contaminant-free surface. Without the occurrence of melting, some other methods of contaminant dispersal are required.

In thermocompression (using heat and pressure only) wire bonding the contaminant dispersal is accomplished by deformation alone[9] and is similar to pressure welding, in which applied pressure and subsequent deformation breaks up the oxide layer.[10] When a metal is irradiated with ultrasonic energy, the yield stress decreases, and this is known as the ultrasonic softening effect.[11] According to the deformation theory of wire bonding, the ultrasonic energy only acts to increase the amount of deformation.[7,12] However, this was shown to be an overly simplified view of the effects of ultrasonic energy, as Zhou *et al.*[13] demonstrated that bonds made with the same amount of deformation with and without ultrasonic energy demonstrated different bond strengths and amounts of bonding. Clearly, this result shows that ultrasonic energy contributes additional effects in ultrasonic bonding besides increased deformation. A study on thermosonic gold ball bonding by Mayer,[14] incorporating *in-situ* microsensors for measuring stress and temperature, showed that relative motion at the ball/substrate interface is important in bond formation; when no sliding occurred, there was no bonding.

I. LUM, Graduate Student, J.P. JUNG, Visiting Professor, and Y. ZHOU, Canada Research Chair in Microjoining, are with the Deparment of Mechanical Engineering, University of Waterloo, Waterloo, ON, Canada. Contact e-mail: nzhou@uwaterloo.ca J.P. JUNG's permanant address is with the Department of Materials Science and Engineering, University of Seoul, Seoul, 130-743, Korea.

Manuscript submitted August 9, 2004.

In thermosonic wire bonding, it is the dynamic force supplied by the ultrasonic transducer that causes the bonding tip and, hence, the ball/substrate faying interface to move in a reciprocating motion. The amplitude of the bonding-tip oscillation is proportional to the ultrasonic power applied.[15] The relative motion experienced when the ball is sliding will lead to wear of material (or contaminant) according to an equation developed for contacting surfaces in relative motion:[16]

$$t = d\frac{H}{K}\frac{1}{PV} \qquad [1]$$

where t is the time required, d is the depth of material worn, P is the mean or nominal pressure, H is the hardness of the material, K is the wear-coefficient constant, and V is the sliding velocity. This wear of material is termed fretting when small-amplitude oscillations are involved. A sufficient removal of the contaminant layer is required for bonding to occur between the underlying metal surfaces.

In thermosonic wire bonding, the bonding force and ultrasonic vibration are applied to the ball/substrate combination by the bonding tool. The ball/substrate situation may be simplified as a contact pair under both normal and tangential forces, which has been extensively studied.

Mindlin[17] studied the compliance of two perfectly elastic spheres subjected to both normal force (N) and tangential force (S). When the spheres are brought into contact under normal force (N), the contact area is over a circle of radius a and is proportional to $N^{1/3}$. Gross sliding on a macroscopic scale initiates when the tangential force exceeds a critical value of $\mu_s N$, where μ_s is the coefficient of static friction. On the other hand, with application of tangential force less than the critical value, a shear traction (q) is introduced over the contact area. Mindlin showed that the traction would rise to infinity at the periphery if no slip occurred and, obviously, this infinite traction force is not attainable. Therefore, the contacting material at the periphery will have to undergo slip to relieve the stress, and this slip, on the order of 0.25 to 2.5 μm,[18] is termed "microslip."

Mindlin[17] provided an equation to calculate the size of the microslip region at the periphery (Figure 1(a)):

$$a' = a\left(1 - \frac{S}{\mu_s N}\right)^{\frac{1}{3}} \qquad [2]$$

where N is the normal force, S is the tangential force, μ_s is the coefficient of static friction, a' is the annulus inner radius, and a is the contact radius. Therefore, the microslip region covers an annulus, $a' < r < a$, while no slip occurs over the circle of radius a' (the stationary region). The microslip annulus grows inward with increasing tangential force up to the point of gross sliding, at which point the microslip annulus has grown to the center of the contact circle, as shown in Figure 1(b).

A study by Johnson[19] on the effect of oscillating tangential forces on the surface of a metal plate in contact with a metal sphere lends support to Mindlin's microslip theory.[17] Johnson showed that before the onset of gross sliding, a fretted annulus due to microslip was observed on the surface of the plate. As the magnitude of the tangential force was increased, the inner radius of the annulus grew inward until it reached the center at the point of gross sliding. However, comparable studies/observations in wire bonding applications have not been reported.

II. EXPERIMENTAL METHODS

25 μm diameter gold wire (AW8) manufactured by K&S Bonding Wire (WillowGrove, PA) was used to ball bump on 1-mm-thick OFHC copper substrates supplied by Good Fellow Corporation (Huntingdon, England). The substrates were metallographically polished with Al_2O_3 up to a surface finish of 0.05 μm prior to bonding, so that the surface roughness would be similar to that on thin-film bond pads. The

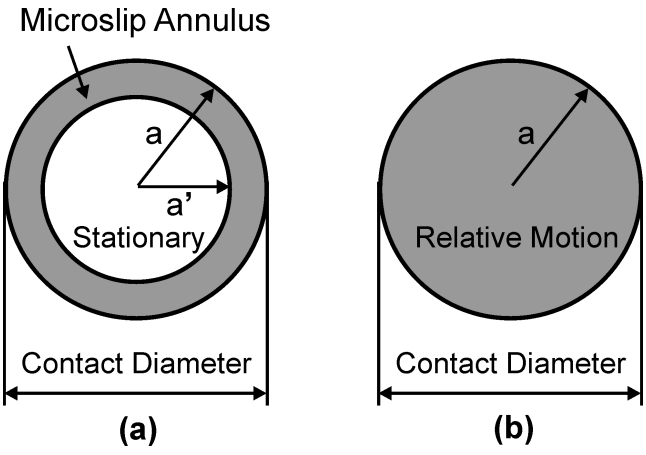

Fig. 1—(a) Stationary and microslip regions in a circular contact undergoing microslip and (b) circular contact showing area undergoing relative motion on the verge of gross sliding ($a' = 0$) and during gross sliding.

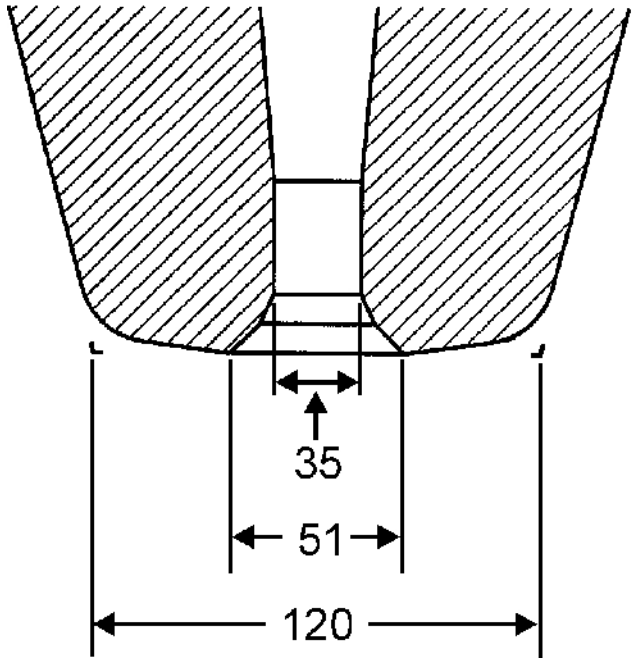

Fig. 2—Capillary geometry used in the study [Figure modified from Ref. 20], all dimensions in micrometers.

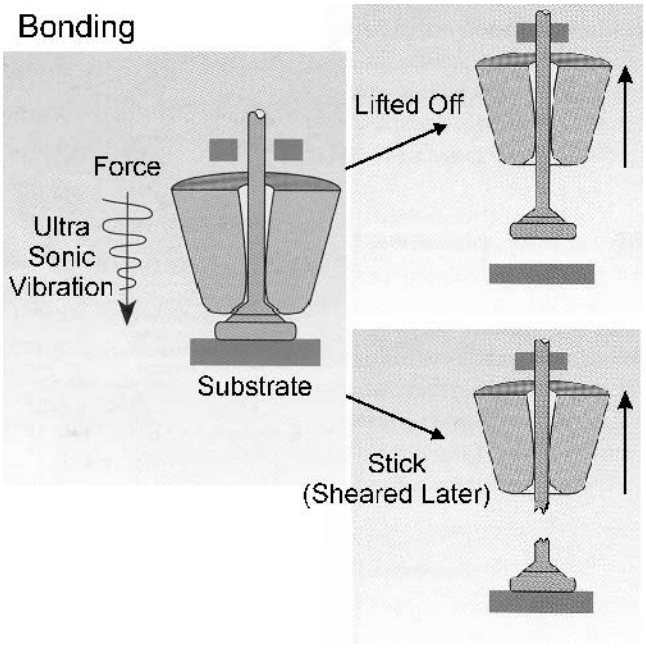

Fig. 3—The two types of bonding outcomes resulting in footprints (Figure modified from Ref. 21).

capillary used was a Small Precision Tools part SBNE-35ED-AZM-1/16-XL, with the geometry as shown in Figure 2.

Gold ball bumping was performed on a Kulicke & Soffa 4524D ball bonder (60 kHz ultrasonic frequency) with the copper substrate at ambient temperature. Various parametric conditions were selected, and ten bonds were made at each combination of parameters. The normal bonding forces used were low, medium, and high forces of 35, 80, and 110 gf, respectively, with the bonding time held constant at 1000 ms. In the following discussion, one representative bond has been selected from each group of ten bonds made at the same set of parametric conditions.

In order to facilitate a more detailed understanding of bonding mechanisms, bond footprints were examined. Two types of bonding outcomes were obtained: lifted off and sticking, resulting in lifted off and sheared footprints, respectively, as shown in Figure 3. If the bond was weak, it would result in a lifted-off footprint on the substrate surface. This would occur in the final step of the bond cycle (wire break) if the wire did not break, but, instead, lifted the ball off at the bond interface because the bond was weaker than the wire. On the other hand, if the bond was stronger than the wire, the ball would remain on the substrate (sticking) when the wire was torn and would, subsequently, be sheared with a DAGE 4000 shear tester at a tool height of 3 μm to obtain the sheared footprint.

The bond quality could be categorized by a simple sorting model, with lifted-off ball bumps characterized as poor quality and bumps remaining on the substrate (sticking) characterized as better quality. The morphological features of the bond footprints were examined using SEM. The presence of fractured microwelds in the footprint indicated metallurgical bonding and could be identified by the presence of gold left from the wire. The distribution of the bonded and/or fretted areas aided in the understanding of the bonding mechanisms.

Table I. Number of Bonds Lifted Off

Bonding Power [mW]	Normal Bonding Force [gf]		
	35	80	110
0	10	10	
130	10	10	10
260	0	10	10
390	0	10	10
520		1	10
650		0	0

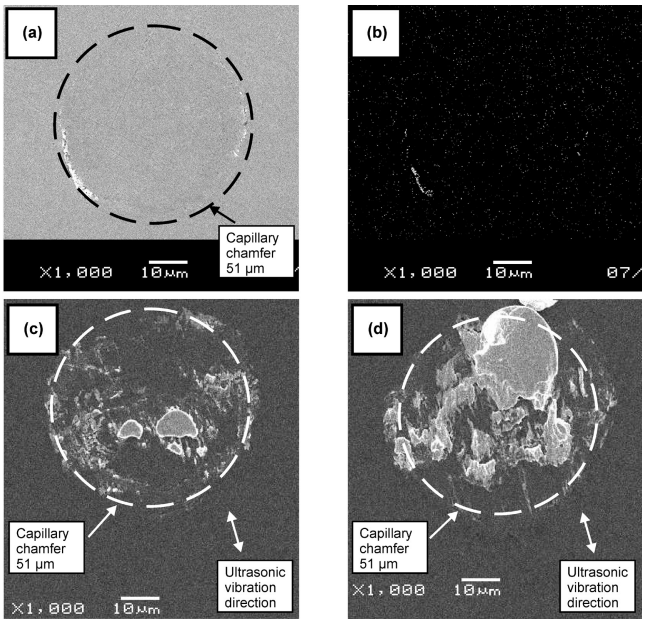

Fig. 4—Bond footprints made with a 35 gf normal bonding force at various bonding powers: (*a*) lifted-off bond footprint made at 130 mW and (*b*) backscattered image of same bond showing gold (bright areas). Sheared footprints made at (*c*) 260 mW and (*d*) 390 mW, noting the directionality of bonding, which is in the ultrasonic vibration direction.

III. RESULTS

A. *Bonds Made with Low Bonding Force*

An earlier bond development study[5] found that at a normal bonding force and bonding-time settings of 35 gf and 1000 ms, respectively, optimum bonds (based on bond shear force) were made. Therefore, the effect of varying power at these settings was examined. In these results, it should be remembered that the capillary chamfer diameter is 51 μm and is clearly indicated in the following figures.

At a 0 mW bond power, no fretting was observed and all ten bonds lifted off, as tabulated in Table I. When the bonding power was increased to 130 mW, all ten bonds lifted off during bonding; however, peripheral fretting at the contact diameter was seen in all bonds of this group, and a typical footprint is shown in Figure 4(a) as a secondary-electron image. Figure 4(b) is the backscattered electron image of the same footprint shown in Figure 4(a). In backscattered electron imaging, gold shows up as bright areas compared to the copper, which appears darker since gold has a higher atomic density than copper. It can be seen that there was bonding in the peripheral area, indicated by the transfer of gold onto the substrate.

However, not all of the bright areas in the secondary-electron image (Figure 4(a)) were identified as gold in the backscattered electron image (Figure 4(b)), which indicates that there were areas on the substrate contacted by the ball which underwent a change in surface morphology but did not have adherent gold upon observation after bonding. In the areas where it appeared bright in the secondary-electron image (Figure 4(a)) but not correspondingly so in the backscattered electron image (Figure 4(b)), there may have initially existed gold bonding, but when the ball lifted off, the gold would have remained completely on the gold ball and not the substrate. There is also the possibility that no gold bonding ever occurred in those areas because of insufficient contaminant removal. Despite the limitations of the foregoing discussion, it can still be concluded that the bright areas in secondary imaging may indicate the occurrence of fretting and that these fretted areas may or may not result in bonded areas as indicated by the presence of gold. It appears from Figure 4(a) that there existed a fretted-annulus inner diameter (i.d.) of about 45 μm, with a fretted-annulus outer diameter (o.d.) of about 49 μm (Table II).

With an increase of bonding power to 260 mW, stronger bonding was seen, as none of the bonds lifted off during bonding (Table I). Figure 4(c) shows a sheared fracture surface of a ball bump made at 260 mW that remained on the substrate surface. Bonded areas may be seen across the entire footprint surface including the center area, whereas this was not observed for the lower-power bonds (Figure 4(a)). It was also observed that there was localized bonding at the chamfer diameter. Some of the bonded areas in Figure 4(c) appeared to be elongated in the ultrasonic vibration direction. The o.d. increased to about 56 μm (Table II), but the i.d. was now difficult to demarcate due to the large bonding across the entire footprint surface.

At the highest bonding power used (390 mW), once again, none of the bonds lifted off during bonding. A sheared-bond footprint made at 390 mW is shown in Figure 4(d), and the measured o.d. increased to about 61 μm. There also appeared to be more bonded area compared to the bonds made at the lower power (Figure 4(c)).

B. *Bonds Made with Higher Bonding Forces*

The effect of bonding power was then investigated for a higher normal bonding force of 80 gf. At a power of 0 mW, no fretting or bonding was observed and all ten bonds lifted off (Table I). At a slightly higher bonding power of 130 mW, all ten bonds lifted off. Almost no bonded regions were observed as well as no center bonding, as shown in Figure 5(a). This is in contrast to the bonds made at the same power with the low bonding force (Figure 4(a)), in which there was more bonding. The i.d. was about 56 μm, which was larger than that seen in the previous lower-force bonds made at the same bonding power (about 45 μm), with the o.d. measured to be about 56 μm (Table II). The corresponding lifted-off ball underside was measured at the flattened area (i.e., the surface in contact with the substrate during bonding) to be about 58 μm in diameter, as shown in Figure 5(a), and compares well with the o.d. of the footprint of about 56 μm.

When the power was increased to 260 mW, all ten of the bonds still lifted off. This is in contrast with the bonds made at the low bonding force, which had all ten bonds stick at this power. Thus, it is clear that with increased normal bonding force while maintaining a constant bond power, the number of lifted-off bonds increased. An i.d. of about 58 μm with an o.d. of about 69 μm was measured from the footprint obtained at 260 mW, as shown in Figure 5(b), and no bonding was visible in the center area. The i.d. was similar to that at the lower power of 130 mW. However, the o.d. was larger than that obtained at 130 mW. The corresponding lifted-off ball underside was measured at the flattened area to be about 70 μm in diameter, as shown in Figure 5(b). This again compares well with the o.d. of the footprint of about 69 μm.

At a power of 390 mW, once again, all ten bonds lifted off; however, there was a change in the appearance of the footprint morphology (Figure 5(c)). Bonding in the center area was now observed, whereas at the lower bond powers, there was no bonding in the center (Figures 5(a) and (b)). The onset of bonding in the center area occurred at this power (390 mW), compared to a lower power of 260 mW at the low bonding force. The i.d. reduced to about 51 μm while the o.d. increased to about 78 μm and compares well with the diameter of the flattened area of the corresponding lifted-off ball of about 79 μm.

At an increased power of 520 mW, the number of lifted-off bonds reduced to one. As shown in the sheared footprint of Figure 5(d), the i.d. was slightly smaller than the chamfer diameter (51 μm) at about 49 μm, with an o.d. of about 85 μm, and bonding was visible in the center of the footprint. At the highest bonding power used of 650 mW, bond sticking for all of the bonds was achieved. As shown in Figure 5(e), the i.d. was about 47 μm, with an o.d. of about 90 μm, and bonding in the center was quite visible.

Finally, the effect of bonding power was investigated for the highest normal bonding force of 110 gf. The footprints are shown in Figure 6 and continued the trends observed at lower bonding forces. For example, increasing the normal bonding force increased the bonding power required for bond sticking, from 260 to 520 and to 650 mW when the bonding force increased from 35 to 80 and to 110 gf, respectively (Table I). Similarly, the ultrasonic power for the onset of bonding in the central region increased from 260 to 390 and to 520 mW (Figures 4 through 6). The footprint o.d. also continued to increase as the bonding force increased (Table II) for a constant bonding power.

At the higher normal bonding forces of 80 and 110 gf at higher bonding powers (Figures 5(d) and (e) and Figure 6(e)), there existed a very pronounced annular bonded area extending

Table II. Fretted Annulus Inner and Outer Diameters [μm]

Bonding Power [mW]	Normal Bonding Force [gf]					
	35		80		110	
	ID	OD	ID	OD	ID	OD
0	N/A	N/A	N/A	N/A		
130	45	49	56	56	60	60
260	N/A	56	58	69	66	71
390	N/A	61	51	78	61	82
520			~49	85	51	88
650			~47	90	~45	91

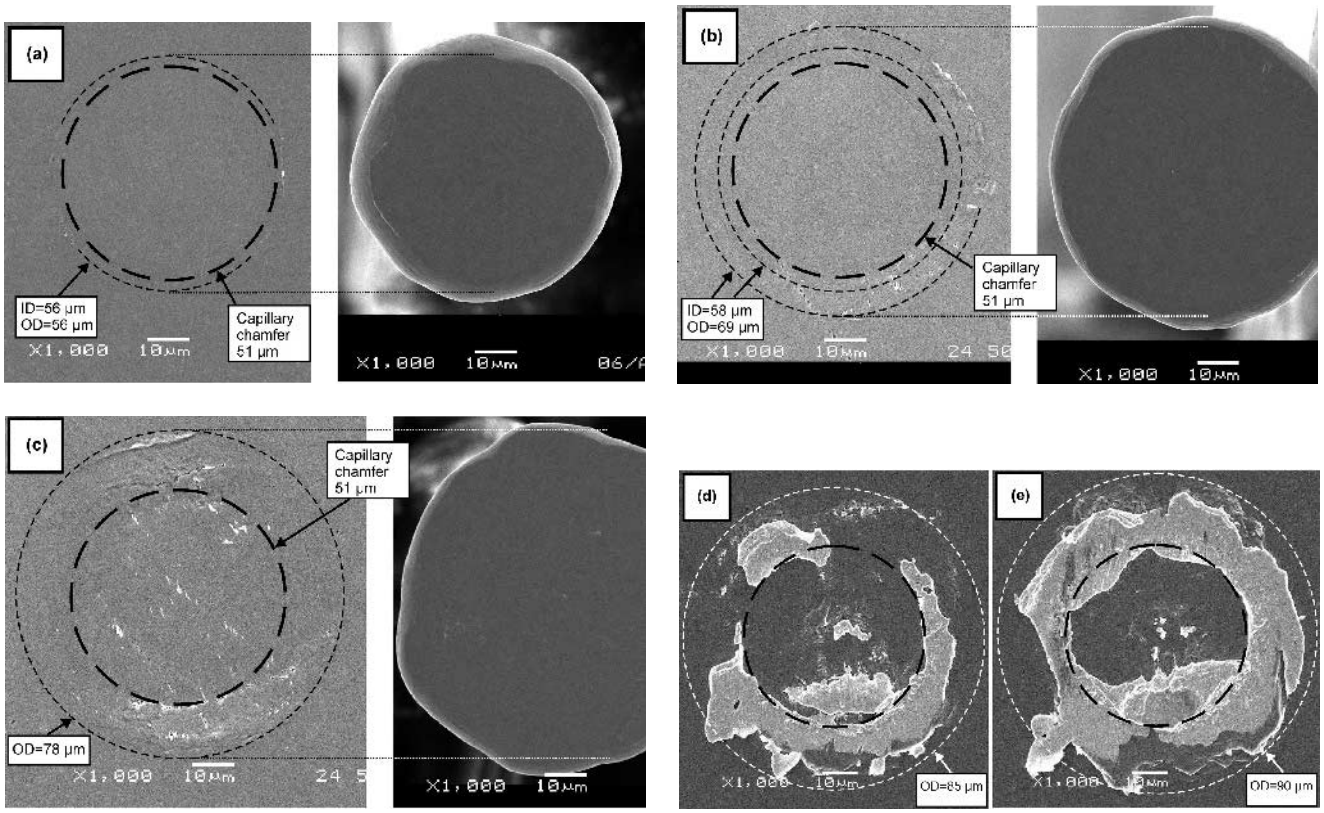

Fig. 5—Bond footprints made with an 80 gf normal bonding force at various bonding powers. Lifted-off bond footprints made at (*a*) 130 mW, (*b*) 260 mW, and (*c*) 390 mW paired with each corresponding lifted-off ball showing the same contact diameter as the o.d.. Sheared footprints made at (*d*) 520 mW and (*e*) 650 mW.

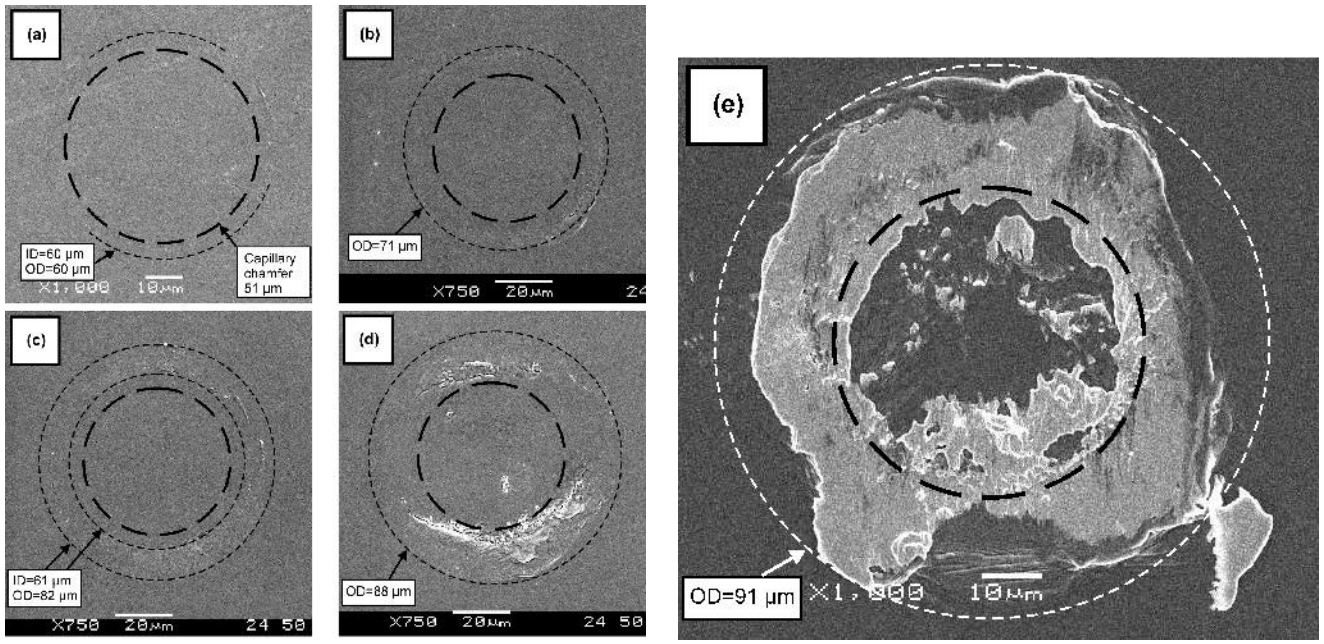

Fig. 6—Bond footprints made with a 110 gf normal bonding force at various bonding powers. Lifted-off bond footprints made at (*a*) 130 mW, (*b*) 260 mW, (*c*) 390 mW, and (*d*) 520 mW. Sheared-bond footprint made at (*e*) 650 mW.

from the capillary chamfer diameter to the contact periphery. On the other hand, at the lower normal bonding force of 35 gf (Figures 4(c) and (d)), the annular bonded area was not as pronounced. Therefore, it can be concluded that with increased normal bonding force, the annular bonded area becomes more pronounced.

IV. DISCUSSION

A. *Bond Development*

With an increasing tangential force, a transition from microslip to gross sliding will occur (Figure 1), as predicted by Mindlin's microslip theory for two perfectly elastic spheres pressed together by a normal force.[17] However, this classical theory needs to be modified, by taking into consideration the large ball deformation and complex bonding-tool geometry, to explain the general phenomena observed in the evolution of bond footprints in this work. Such a model is shown in Figure 7 to illustrate the morphology of the footprint transitioning from microslip to gross sliding as the ultrasonic power (tangential force) increases. The details of this model are discussed in the following text with regard to the experimental observations at an 80 gf normal bonding force, but are also applicable to the other bonding forces in this study.

At low ultrasonic power, microslip initiated at the periphery of the ball/substrate contact and the microslip annulus was thin, as shown in Figure 7(a), with a shaded annulus indicating the fretted region. The crosshatching indicates the density of bonding. This low-power situation was observed for the bonds made at 130 mW, in which evidence for microslip initiation at the periphery was provided by the equivalence of the flattened area on the lifted-off ball underside (about 58 μm in diameter) with the o.d. of the footprint (about 56 μm).

As the power increased to 260 mW (Figure 7(b)), the i.d. of the microslip annulus decreased, as predicted by Eq. [2]. At the same time, the o.d. increased from about 56 μm in Figure 5(a) to about 69 μm in Figure 5(b) when the power increased from 130 to 260 mW. The increase in the o.d. is attributed to the increased ball deformation due to the increased ultrasonic softening effect at increased power.

With a further increase of power to 390 mW, the fretted area extended to cover the entire ball/substrate contact area and entered the gross-sliding regime (observed in Figure 5(c) and shown schematically in Figure 7(c)). However, extensive bonding appeared to stop around the chamfer diameter of 51 μm, with only a few distinct bonded pieces in the center area. This geometry differs from that predicted by classical microslip theory for gross sliding (Figure 1(b)). This discrepancy is believed to be caused by a complex distribution of the normal stress at the ball/substrate interface, with the highest normal stress in a ring at about the chamfer diameter of 51 μm and decreasing to a local minimum at the center (Figure 8). This stress distribution is suggested based on a numerical calculation of the stress distribution in the substrate under a ball bond (Figure 9).[14] The lower normal stress at the center area would lead to less material removal in relative sliding, as given by Eq. [1], as compared to the areas under the chamfer diameter and capillary shoulder. Therefore, bonding is more likely to occur in those areas with a higher normal stress.

Once in the gross-sliding regime, with increased bonding power, the i.d. appeared to remain at about 51 μm (Figures 5(c) through (e)), due to the complex stress distribution at the

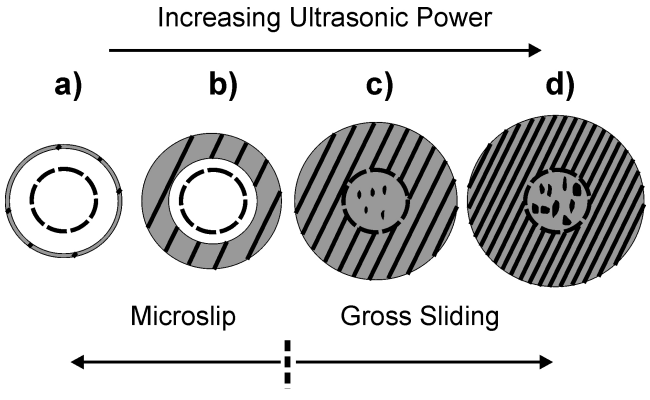

Fig. 7—Schematic illustration of the change in footprint morphology from microslip to gross sliding for increasing ultrasonic power. Gray areas indicate fretting, while the dashed circle indicates the capillary chamfer diameter. Bonding density is indicated by the crosshatching.

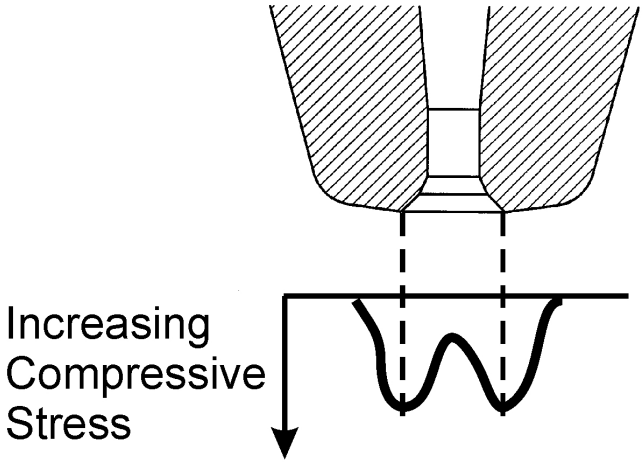

Fig. 8—Suggested normal stress distribution at the ball/substrate interface (modified from Ref. 20).

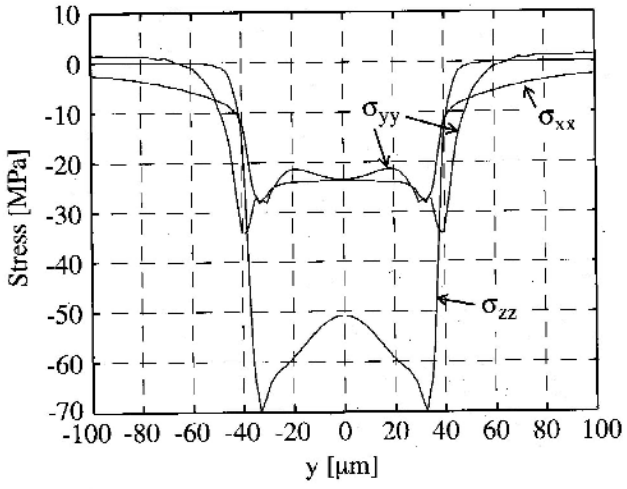

Fig. 9—Stress distribution for ball bonding at a point 4 μm below the substrate surface, calculated using finite-element methods. The term σ_{zz} is the normal stress distribution.[14]

ball/substrate interface previously discussed. However, the density of bonding increased with increased bonding power, and, in fact, is true for the range of results studied. The increased bonding density is a result of the increased fretting due to the increased displacement (as shown by Eq.[1]) during relative motion at the ball/substrate interface with increased power.

B. *Effect of Bonding Force*

Figure 10 shows the percent lifted off vs bonding power for the three normal bonding forces used, and it is indicated in the figure where the microslip or gross-sliding (shaded area) regime was active by the hollow and filled-in symbols, respectively. It can be seen that the bonding-regime transition line shifts toward higher powers with increased normal bonding force, which is consistent with Eq. [2]. With increased normal force, in order to achieve sliding, the tangential force also must be increased. Hence, the ultrasonic power needs to be increased at a higher normal bonding force in order to transition into the gross-sliding regime.

It can also be seen from Figure 10 that the bonds made at the increased normal bonding force required higher power to achieve lift-off rates equal to the bonds made at the lower bonding force, which can be explained based on the growth of the microslip region. The bonds made at the medium bonding force (80 gf) did not achieve gross sliding until a bonding power of 390 mW, while bond sticking did not occur until 520 mW. Below 390 mW, microslip was confined to the outside contact diameter of the ball/substrate interface and the bonded area was low, resulting in lifted-off bonds. On the other hand, bonds made with a lower normal bonding force of 35 gf were shown to be in the gross-sliding regime at a lower bonding power of 260 mW. As a result, more bonding occurred with bonds made at a 35 gf normal bonding force compared to both of the higher normal bonding forces at similar low powers.

It was also observed that with increased normal bonding forces, the bonding at the chamfer diameter in the form of an annulus became more pronounced. This is believed to be due to the stress distribution which arose from the capillary geometry being more effectively transmitted to the ball/substrate interface with increased normal bonding forces.

In summary, an increased bonding power is required for an increased normal bonding force in order to transition the bonding from microslip into gross sliding and, hence, increase the bonded area. This observation agrees well with what is often encountered in industry, in that an increased normal bonding force requires an increased bonding power in order to achieve adequate bond strength.[22]

It should be noted that these studies were all performed on bulk copper substrates. In most industrial practice, bonds are made to thin-film copper metallization. These results may not be fully applicable to the thin-film situation, since thin films may have a different mechanical behavior and also introduce other complexities. For instance, with a higher applied ultrasonic bonding power, delamination of the thin film may occur. Also, when a higher ultrasonic bonding power is combined with higher normal bonding forces, cratering of the underlying silicon may occur. However, it is believed that the results and discussions on the mechanism of bond formation should be generally applicable, regardless of substrate thickness.

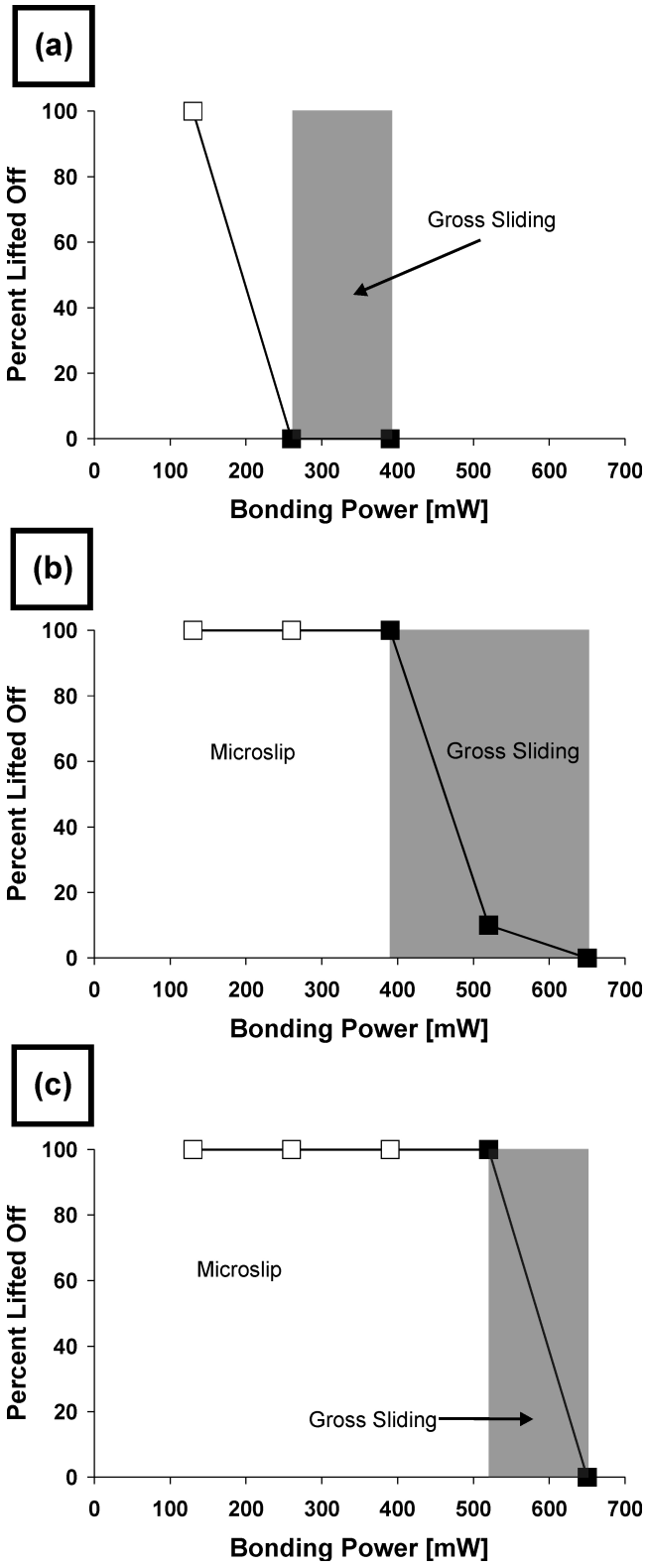

Fig. 10—Percent lifted off vs bonding power for normal bonding forces of (*a*) 35 gf, (*b*) 80 gf, and (*c*) 110 gf. Hollow symbols indicate a microslip condition, while solid symbols indicate gross sliding. Shaded area indicates a gross-sliding regime.

V. SUMMARY AND CONCLUSIONS

Ultrasonic gold ball bumps were made on copper substrates at ambient temperature over a range of bonding parameters of ultrasonic power and bonding force. The evolution of the bond-footprint morphologies left on the copper substrate was studied in detail with SEM. The major findings from this study are summarized as follows.

1. A model was developed based on classical microslip theory to explain the general phenomena observed in the evolution of bond footprints during ultrasonic ball-wire bonding. The specific effects of ultrasonic energy and complex stress distributions arising from tool geometry must be taken into consideration.
2. Relative motion at the bond interface exists as either microslip or gross sliding, depending on the ultrasonic power level and the normal bonding force used. For a given normal bonding force, at lower powers, the bonding is in the microslip regime and, with increased power, transitions into gross sliding.
3. An increased normal bonding force shifts the transition line for gross sliding toward higher bonding powers, which indicates that for an increased normal bonding force, a higher power is required to obtain satisfactory bonding.
4. While increased ultrasonic power grows the microslip region toward the ball center, it also increases the contact diameter (due to the increased ultrasonic softening) and, hence, the microslip annulus o.d.
5. The bonded areas observed during gross sliding in ball bonding differ from those observed for the sphere-on-plate experiment, due to the complex capillary geometry. As a result, localized bonding occurs in areas where stress concentrations exist arising from the capillary geometry. This capillary-geometry effect on localized bonding is more pronounced with increased normal bonding forces.

ACKNOWLEDGMENTS

This work has been supported by the Canada Research Chairs Program (www.crc.gc.ca) and the Natural Sciences and Engineering Research Council (NSERC) of Canada (www.nserc.ca).

REFERENCES

1. G.G. Harman: *Wire Bonding in Microelectronics—Materials, Processes, Reliability, and Yield,* 2nd ed., McGraw-Hill, New York, NY, 1997, pp. 1-23.
2. J. Rohan, G. O'Riordan, and J. Boardman: *Appl. Surface Sci.,* 2002, vol. 185, pp. 289-97.
3. C.C. Lee *et al.*: *Proc. SPIE—Int. Soc. Opt. Eng.,* 2001, vol. 4587, pp. 511-14.
4. R. Batra: Master's Thesis, The Ohio State University, Columbus, OH, 1997.
5. I. Lum, N.J. Noolu, and Y. Zhou: *Proc. SPIE—Int. Soc. Opt. Eng.,* 2003, vol. 5288, pp. 130-35.
6. J.E. Krzanowski: *IEEE Trans. Compon. Hybrids Manufacturing Technol.,* 1990, vol. 13, pp. 176-81.
7. G.G. Harman and J. Albers: *IEEE Trans. Parts, Hybrids Packaging,* 1977, vol. PHP-13, pp. 406-12.
8. J.E. Krzanowski and N. Murdeshwar: *J. Electron. Mater.,* 1990, vol. 19 (9), pp. 919-28.
9. Y. Takahashi, S. Shibamoto, and K. Inoue: *IEEE Trans. Compon. Hybrids Manufacturing Technol.,* Part A, 1996, vol. 19 (2), pp. 213-23.
10. H.A. Mohamed and J. Washburn: *Welding J.,* 1975, vol. 54 (9), pp. 302s-310s.
11. B. Langenecker: *IEEE Trans. Sonics Ultrasonics,* 1966, vol. SU-13 (1), pp. 1-8.
12. G.G. Harman and K.O. Leedy: *10th Annual Proc. Reliability Physics,* Las Vegas, NV, IEEE, New York, Apr. 5–7, 1972, pp. 49-56.
13. Y. Zhou *et al.*: *IEEE Transactions on Components and Packaging Technologies,* in press.
14. M. Mayer: Ph.D. Dissertation, Swiss Federal Institute of Technology (ETH), Zurich, 2000.
15. F. Osterwald, K.D. Lang, and H. Reichl: *ISHM '96 Proc.,* Reston, VA, pp. 426-31.
16. *Wear Control Handbook,* ASME, 1980, New York.
17. R.D. Mindlin: *Trans. ASME*, Ser. E, *J. Appl. Mech.,* 1949, vol. 16, pp. 259-68.
18. K.L. Johnson: *Contact Mechanics,* Cambridge University Press, London, 1985.
19. K.L. Johnson: *Proc. Royal Soc. A,* 1955, vol. 230, pp. 531-49.
20. *High-Technology Wire Bonding Tools, Volume 10,* Gaiser Tool Company, Ventura, CA.
21. *Micro-Swiss Capillary Catalog,* Kulicke & Soffa Industries, Inc., WillowGrove, PA.
22. Z.N. Liang, F.G. Kuper, and M.S. Chen: *Microelectron. Reliability,* 1998, vol. 38 (6–8), pp. 1287-91.